Triplet Formation Involving a Polar Transition State in a Well-Defined Intramolecular Perylenediimide Dimeric Aggregate

Dirk Veldman,[†] Stéphanie M. A. Chopin,[†] Stefan C. J. Meskers,[†] Michiel M. Groeneveld,[‡] René M. Williams,[‡] and René A. J. Janssen*[,†]

Molecular Materials and Nanosystems, Eindhoven University of Technology, P.O. Box 513, 5600 MB Eindhoven, The Netherlands, Molecular Photonics Group, Van't Hoff Institute for Molecular Sciences, Universiteit van Amsterdam, Nieuwe Achtergracht 129, 1018 WS Amsterdam, The Netherlands

Received: March 14, 2008; Revised Manuscript Received: April 16, 2008

A cofacially stacked perylenediimide (PDI) dimer with a xanthene linker was studied under a variety of conditions (solvent, temperature) and serves as a model for the molecular interactions occurring in solid films. Intrinsically, the PDI units have a fluorescence quantum yield (Φ_F) close to unity, but Φ_F is lowered by a factor of 6−50 at room temperature when two PDI moieties are held in a cofacial arrangement, while the decay time of the most emissive state is increased significantly ($\tau_F = 27$ ns in toluene) compared to a monomeric PDI molecule ($\tau_F = 4$ ns). Fluorescence measurements show a strong solvent and temperature dependence of the characteristics of the emissive excited state. In a glassy matrix of toluene (TOL) or 2-methyltetrahydrofuran (2-MeTHF), Φ_F is high, and the decay time is long ($\tau_F = \sim 50$ ns). At higher temperature, both Φ_F and τ_F are reduced. Interestingly, at room temperature, Φ_F and τ_F are also reduced with increasing solvent polarity, revealing the presence of a polar transition state. Photoinduced absorption of the stacked molecules from the picosecond to the microsecond time scale shows that after photoexcitation reorganization occurs in the first nanoseconds, followed by intersystem crossing (ISC), producing the triplet excited state. Using singlet oxygen ($^1\Delta_g$) luminescence as a probe, a triplet quantum yield (Φ_T) greater than 50% was obtained in air-saturated 2-Me-THF. Triplet formation is exceptional for PDI chromophores, and the enhanced ISC is explained by a decay involving a highly polar transition state.

Introduction

Enhanced triplet generation following photoinduced charge transfer was recently reported by various groups in electron donor−acceptor polymer blend films that are of interest for application in organic photovoltaic devices.[1] In these electron blend films, intersystem crossing (ISC) is promoted relative to films of the pristine polymers. Little is known about the mechanism of triplet formation from charge-transfer (CT) states in these blends, but it is of importance for polymer photovoltaics because it reduces the lifetime of the CT state that serves as a precursor for free charge carriers.

In molecules such as acetone and, for example, aromatic ketones, known for their high triplet yields, the n−π* transition of the carbonyl group can be viewed as the transfer of charge from the lone pair of the oxygen atom to the carbon atom. This exemplifies the importance of charge transfer in triplet state formation. The orbital magnetic momentum is changed when the interacting orbitals are located in different areas of the space on the molecule, compensating the change of spin magnetic momentum of the electron (spin−orbit coupling).[2]

Previous studies on triplet excited-state population in photoexcited electron donor−acceptor dyads have shown that enhanced ISC can be induced via population of the radical (ion) pair. Two mechanisms of ISC via the radical pair have been proposed, radical pair intersystem crossing (RP-ISC)[3–6] and spin−orbit intersystem crossing (SO-ISC).[3,7] RP-ISC involves a spin dephasing from the initially created singlet radical pair to a radical pair with triplet character ($^1CT \rightarrow {}^3CT$) by hyperfine interactions, followed by a rapid charge recombination into the lowest charge-neutral triplet excited state ($^3CT \rightarrow T_1$). SO-ISC involves a direct charge recombination from the singlet radical pair to T_1 ($^1CT \rightarrow T_1$) with a simultaneous spin inversion via spin−orbit coupling. It is difficult to distinguish between these two mechanisms, but it is observed that the SO-ISC mechanism prevails when strong electronic coupling—requiring a short electron donor−acceptor distance—is present between the two units.[8]

Perylenediimides (PDIs) have been well-studied over the past decades and are often used as model compounds because of their high fluorescence quantum yields, chemical inertness, and photochemical stability. They are well-soluble if "swallow tail" alkyl chains or substituted phenyl rings are introduced.[9] Under direct photoexcitation, the fluorescence quantum yields of PDIs in solution are high ($\Phi_F \geq 95\%$) and their triplet quantum yields are low ($\Phi_F < 0.1\%$ and $\sim 0.5\%$ have been reported).[10] However, the triplet excited state can be populated via energy transfer from other triplet states, and the triplet−triplet (T_1-T_n) absorption spectrum, triplet energy (1.20 ±0.08 eV), and triplet lifetime ($\sim 100\ \mu$s) of PDIs have already been reported by Ford and Kamat in 1987[10] and were recently studied intensively in covalent systems where a perylenediimide is attached to fullerenes or porphyrins.[11]

The organization of conjugated materials on the nanometer length scale has important consequences for their optical properties. The effect of π-stacking of PDI molecules on the optical properties has been studied by changing temperature, solvent, and concentration.[12] Much research has also focused

* To whom correspondence should be addressed. E-mail: r.a.j.janssen@tue.nl.
[†] Eindhoven University of Technology.
[‡] Universiteit van Amsterdam.

10.1021/jp8022524 CCC: $40.75
Published on Web 06/11/2008

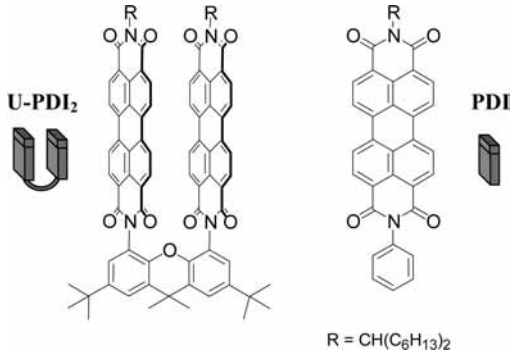

Figure 1. Molecular structures of **U-PDI$_2$**, reference compound **PDI**, and their cartoon-like representations.

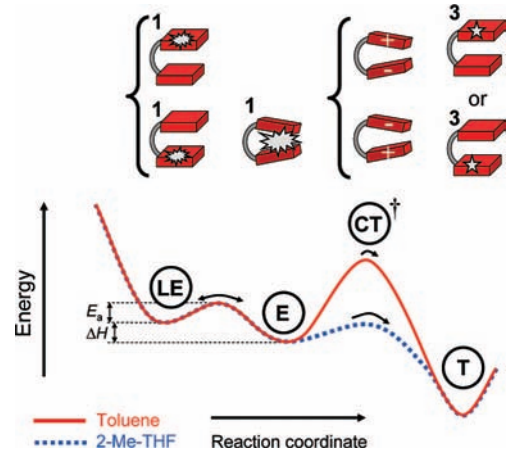

Figure 2. Schematic diagram showing the lowest singlet exciton state (LE), the excimer-like state (E), the highly polar transition or intermediate state (CT†), the localized triplet excited state (T), and the energy barriers between these states in TOL (solid line) and 2-Me-THF (dashed line).

on crystalline films of perylene tetracarboxylic dianhydride (PTCDA), which show many similar optical properties as PDI stacks in solution: broad, unstructured, red shifted emission with relatively long PL (photoluminescence) decay times, different from the single molecules.[13] The emissive properties of crystalline PTCDA films are often described in terms of molecular dimers.

Well-defined covalently linked, cofacially stacked PDI dimers were recently reported[14–17] and are shown to have enhanced blue-shifted absorption compared to the monomers and weak red-shifted emission. In the dyads of Wasielewski et al., the PDI moieties are linked with a xanthene group and are bay-substituted with either pyrrolidine[15] or 3,5-di-*t*-butylphenoxy groups.[16] More recently, also "bare" PDI dimers were presented by the same group.[17] Photoexcitation of the pyrrolidine-substituted dimer in relatively nonpolar toluene (TOL) leads to a fast (τ = 0.52 ps) charge transfer between the two PDI chromophores, creating an intramolecularly stacked $PDI^{+\bullet}-PDI^{-\bullet}$ state that decays to the ground state with τ = 220 ps.[15] The photoinduced electron transfer is enabled by the electron-donating pyrrolidine rings that lower the energy of the CT state below that of the initially created, charge-neutral, singlet excited state.[18] Oppositely, for the phenoxy-substituted and -unsubstituted dimers, decay from the photoexcited states does not involve full charge transfer. Upon photoexcitation, these molecules show excimer-like emission, with PL quantum yields and PL lifetimes in TOL amounting to $\Phi_F = 0.06-0.15$ and τ = 19−23 ns for the phenoxy-substituted and to $\Phi_F = 0.02-0.19$ and τ = 9−29 ns for the nonsubstituted dimer.[16b,17] The lower (higher) PL yields and shorter (longer) lifetimes belong to dimers with linear (branched) solubilizing side chains, whose chromophores are more (less) closely packed.[17] A weak solvent dependence of the emission yield and lifetime in three different solvents was tentatively explained by variations in the radiative rate of the phenoxy-substituted dimers or a heavy atom effect of the solvent.[16b] Triplet excited-state properties of these molecular dimers have not been reported thus far.

Here, we study a U-shaped PDI dimer (**U-PDI$_2$**), with two "bare" PDI moieties held in a cofacial configuration by a rigid xanthene linker (Figure 1) and with 1-hexylheptyl side chains. Because, as mentioned before, photoinduced electron transfer is not observed for similar dimers, **U-PDI$_2$** is an interesting model compound to study the effect of higher-lying CT states on the deactivation of excited states. Specifically, with increasing solvent polarity, CT states are reduced in energy and may facilitate the deactivation of lower-lying excited states.

According to PM3 quantum chemical calculations, the xanthene spacer in **U-PDI$_2$** allows for a distance between the two cofacially arranged PDI units of ∼4.5 Å, with a minimum distance of 4.3 Å for each atom.[17] This is significantly more than the perpendicular distance between two molecules in an α-PTCDA crystal (3.2 Å),[19] although small rotations around the xanthene−imide bonds possibly allow closer contacts between the PDI units.

The coupling of the parallel transition dipoles of the two stacked PDI moieties in **U-PDI$_2$** leads to delocalization of the excited state and changes the band shape of the absorption spectrum.[20] The transition from the ground state to the lowest excited level is only weakly allowed, whereas transitions to higher levels are more strongly allowed. After photoexcitation, the electronic state in the dimer will quickly relax to the lowest singlet exciton state (LE).[17] In the LE state, coupling between the two excited states of the single PDI units makes the emission different from that of the monomer; however, the excitation can be described as a superposition of locally excited states of the two units (Figure 2). Due to the coupling, decay from this excited state is forbidden.

The presence of the carbon and oxygen atoms in between the two phenyl moieties of the xanthene linker and the rotational freedom around the xanthene−imide bonds allow for conformational changes,[21] which may enable the formation of an excited state with the chromophores at a closer separation distance than that in the initially created LE state and with the π-electrons shared over the two PDI units. If this conformation is unstable in the ground state, we can denote the distorted excited state as an excimer-like state (E, Figure 2), resembling an excimer, an electronically excited dimer, "nonbonding" in the ground state.[17] The pyrene dimer is one of the most extensively studied excimers, forming weak excited-state complexes in solution and having very weak CT character in its lowest excited state, as observed from minimal solvatochromic shifts.[22] The lowest triplet excited state of **U-PDI$_2$** (T in Figure 2) is expected to be more strongly localized than the lowest singlet excited states of the molecule because the triplet exciton is not stabilized by exciton coupling as the transition from the singlet ground state to a triplet excited state is forbidden by spin selection rules. We therefore expect very similar properties (triplet energy, triplet lifetime, T_1-T_n absorption) for the triplet of **U-PDI$_2$** compared to those of **PDI**, but the triplet yields, as we will demonstrate, can differ substantially. Although low-energy CT states are unavailable, the stacking of PDI chromophores creates a CT transition or high-energy intermediate

state ($PDI^{\bullet+}$_-$PDI^{\bullet-}$) at energies just above the emissive singlet states (denoted with $CT^{\dagger}$ in Figure 2).

In this contribution, we study the formation and decay of the photoexcited singlet (LE, E) and triplet (T) states using steady-state and time-resolved techniques in a set of solvents of different polarity and at a wide range of temperatures. We provide a detailed analysis of the equilibrium between the LE and E states and demonstrate that intersystem crossing to the T state is enhanced by a nearby CT transition state. Consequently, intersystem crossing occurs much faster and more efficient in the stacked dimer than that in monomeric PDI, especially in solvents with a higher polarity.

Experimental Section

General. All reagents and solvents were used as received or purified using standard procedures. **PDI**,[23] 2,7-di-*t*-butyl-9,9-dimethyl-4,5-xanthenediamine,[24] and *N*-(1-hexylheptyl)perylene-3,4-dicarboxyanhydride-9,10-dicarboximide[25] were synthesized following previously reported procedures. Column chromatography was performed using Merck silica gel 60 (230−240 mesh). ^{1}H NMR and ^{13}C NMR spectra were recorded at room temperature on a Varian Mercury (400 and 100 MHz, respectively). Proton chemical shifts are reported in ppm relative to tetramethylsilane (TMS). Infrared (FT-IR) spectra were recorded on a Perkin−Elmer Spectrum One UATR FT-IR spectrophotometer. MALDI-TOF MS spectra were recorded on a Perspective DE Voyager spectrometer using α-cyano-4-hydroxycinnamic acid or 2-[(2*E*)-3-(4-*tert*-butylphenyl)-2-methylprop-2-enylidene] malononitrile (DCTB) as a matrix. Elemental analyses were carried out using a Perkin−Elmer 2400.

U-PDI$_2$. A mixture of 2,7-di-*t*-butyl-9,9-dimethyl-4,5-xanthenediamine (40 mg, 0.113 mmol), *N*-(1-hexylheptyl)perylene-3,4-dicarboxyanhydride-9,10-dicarboximide (215 mg, 0.374 mmol), imidazole (115 mg), and pyridine (10 mL) was heated to 85 °C for 72 h. The crude product was purified by silica gel column chromatography (CH_2Cl_2/ethyl acetate: 7/0.4) to give to give **U-PDI$_2$** as a red−orange solid (135 mg, 81%). IR: ν (cm^{-1}) 1698 and 1657 ($\nu_{C=O}$ imide); ^{1}H NMR ($CDCl_3$, 400 MHz): δ 8.40−7.80 (m, 16H), 7.57 (d, J = 2.4 Hz, 2H), 7.04 (d, J = 2 Hz, 2H), 5.06 (m, 2H), 2.40−0.60 (broad signals), 1.83 (s, 6H), 1.55 (s, 18H); MALDI-TOF MS (*m*/*z*) calcd for $C_{97}H_{98}N_4O_9$ = 1462.73, found $[M^{\bullet}]^+$ = 1462.4. Anal. calcd: C, 79.59; H, 6.75; N, 3.83; found: C, 78.53; H, 6.81; N, 3.82.

Electrochemistry. Cyclic voltammograms were recorded in an inert atmosphere with 0.1 M tetrabutylammonium hexafluorophosphate ($TBAPF_6$) in dichloromethane (DCM) as the supporting electrolyte. The working electrode was a platinum disc (0.2 cm^2), and the counter electrode was a platinum electrode. The scan was performed using a Ag/AgCl reference electrode with a ferrocene−ferrocenium couple (Fc/Fc^+) as an internal standard (+0.35 V vs. Ag/AgCl in DCM) using a μAutolab II with a PGSTAT30 potentiostat and a scan speed of 100 mV/s. Deconvolution to remove diffusion phenomena and to have sharper curves was performed mathematically with the Autolab software.[26]

Absorbance and Fluorescence. The solvents for spectroscopic studies were spectroscopic-grade and air-equilibrated, unless stated otherwise. UV/vis absorption spectra were recorded using a Perkin−Elmer Lambda 900 spectrophotometer, and steady-state fluorescence spectra were recorded on an Edinburgh Instruments FS920 double-monochromator spectrophotometer with a Peltier-cooled red-sensitive photomultiplier. The emission spectra were corrected for the wavelength dependence of the sensitivity of the detection system. Time-correlated single-photon counting fluorescence studies were performed on an Edinburgh Instruments LifeSpec-PS spectrometer by photoexcitation with a 400 nm picosecond laser (PicoQuant PDL 800B) operated at 2.5 MHz and detection with a Peltier-cooled Hamamatsu microchannel plate photomultiplier (R3809U-50). The data were deconvoluted with the instrument response function of the instrument, recorded using dispersed light, and fitted to a multiexponential function using the Fluofit package (PicoQuant, Berlin). Low-temperature (< 300 K) fluorescence was recorded using an Oxford Instruments nitrogen flow (CF) cryostat connected to an Oxford ITC601 temperature controller. A Lauda RC 20 CS refrigerated bath circulator was used to measure at temperatures above 300 K. The samples were allowed to equilibrate for 15 min at each temperature.

Subpicosecond Pump−Probe Photoinduced Absorption (ps-PIA). Experiments were performed with a Spectra-Physics Hurricane Titanium:Sapphire regenerative amplifier system. The full spectrum setup was based on an optical parametric amplifier (Spectra-Physics OPA 800C) as the pump. The residual fundamental light, from the pump OPA, was used for white-light generation, which was detected with a CCD spectrograph (Ocean Optics). The polarization of the pump light was controlled by a Berek polarization compensator (New Focus). The Berek polarizer was always included in the setup to provide the magic-angle conditions. The probe light was passed over a delay line (Physik Instrumente, M-531DD) that provides an experimental time window of 1.8 ns with a maximal resolution of 0.6 fs/step. The OPA was used to generate excitation pulses at 530 nm. The laser output was typically 3.5−5 μJ $pulse^{-1}$ (130 fs FWHM) with a repetition rate of 1 kHz. The samples were placed into cells of 2 mm path length (Hellma) and were stirred with a downward projected PTFE shaft using a direct drive spectro-stir (Spectrocell). This stir system was also used for the white-light generation in a 2 mm water cell. For femtosecond transient absorption in the NIR region, a Control Development NIR-256L-1.7T1-USB optical spectrometer system, InGaAs detector with 512 element arrays responding to a wavelength range from 900 to 1700 nm, was used. Detection light was generated with a sapphire plate. See the Supporting Information of ref 11 for optical layout.

Nanosecond Pump−Probe Photoinduced Absorption (ns-PIA). Spectra were recorded by exciting the sample with pulses at 488 nm (pulse width 4 ns, repetition rate 10 Hz) obtained from an optical parametric oscillator (OPO), pumped by the third harmonic of a Nd:YAG laser. An intensified charge-coupled device (CCD) camera was used to record the transmission of a tungsten−halogen probe light through the sample after dispersion by a spectrograph. The signal acquisition by the CCD camera was electronically gated at different time delays after the excitation pulse. To obtain differential transmission spectra, the reference transmission was recorded at a 20 ms delay. For the ns-PIA experiments, oxygen- free solutions were prepared in a glovebox ($[O_2]$ < 5 ppm), unless stated otherwise.

Near-Steady-State Photoinduced Absorption (ss-PIA). Spectra were recorded between 0.35 and 2.5 eV by excitation at either 488 nm or at 351 + 364 nm with a mechanically modulated (275 Hz) cw argon ion laser pump beam and by measuring the change in transmission of a tungsten−halogen probe beam through the sample (ΔT) with a phase-sensitive lock-in amplifier after dispersion with a monochromator and detection using Si, InGaAs, and cooled InSb detectors. The pump power was 25 mW, with a beam diameter of 2 mm. The PIA signal ($-\Delta T/T$) was corrected for the photoluminescence, which was recorded in a separate experiment. Samples were

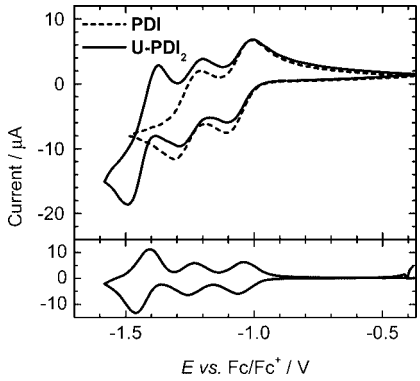

Figure 3. Cyclic voltammograms of **PDI** and **U-PDI$_2$** in DCM. The bottom panel shows the deconvoluted voltammogram of **U-PDI$_2$**.

held in a screw-capped cell (1 mm, Spectrocell) at 295 K or cooled using an Oxford Instruments nitrogen flow (CF) cryostat connected to an Oxford ITC601 temperature controller.

Oxygen Phosphorescence. For the singlet oxygen ($^1\Delta_g$) phosphorescence measurements, the spectra were recorded by exciting the sample with the second harmonic of a Nd:YAG laser (5 ns, 532 nm, 10 Hz rep. rate). The incoming beam was filtered with a 532 nm laser line filter (Lot Oriel), and the luminescence was collected at a straight angle to the excitation beam with a liquid-N_2-cooled ultrasensitive germanium detector (Edinburgh Instruments EI-P) with an RG1000 (Schott) glass filter and a 1292 nm NIR band ($T = 60\%$ at 1270 nm, FWHM = 80 nm) pass filter (Lot Oriel). The diode signals were transferred to a PC and averaged 96 times. The samples were air-saturated solutions with absorbances amounting to 0.35 ± 0.01 at 532 nm in a quartz cell with an optical path length of 10 mm.

Results

A. Synthesis of U-PDI$_2$. The cofacially stacked dimer **U-PDI$_2$** was synthesized by heating a solution of 2,7-di-*t*-butyl-9,9-dimethyl-4,5-xanthenediamine and *N*-(1-hexylheptyl)perylene-3,4-dicarboxyanhydride-9,10-dicarboximide in imidazole and pyridine to 85 °C for 72 h, followed by purification by column chromatography. As a result of its branched solubilizing 1-hexylheptyl tails at the ends of the two chromophores, **U-PDI$_2$** is very soluble in a wide range of organic solvents, allowing detailed characterization and analysis of its photophysical properties.

B. Electrochemistry. The cyclic voltammogram of **U-PDI$_2$** in dichloromethane (DCM) shows three reduction peaks (Figure 3). On the basis of the deconvoluted voltammogram showing a 1:1:2 pattern for the current, we propose that first one and then the other PDI unit is reduced, first creating the monoanion (PDI−PDI$^-$) at −1.05 V, followed by the dianion (PDI$^-$−PDI$^-$) at −1.24 V and the tetraanion (PDI^{2-}−PDI^{2-}) at −1.42 V versus Fc/Fc$^+$.[27] Comparison with **PDI**, having reduction potentials of −1.05 V for the monoanion (PDI$^-$) and −1.25 V for the dianion (PDI^{2-}), indicates a minimal effect of the stacking on the first reduction potential of the PDI moieties in **U-PDI$_2$**. The formations of the dianion (PDI$^-$−PDI$^-$) and tetraanion (PDI^{2-}−PDI^{2-}) occur at more negative potentials as a result of Coulomb repulsion with the other negatively charged chromophore. The oxidation of **U-PDI$_2$** occurs at a similar potential as that for **PDI** and is estimated at +1.23 V versus Fc/Fc$^+$ (Supporting Information, Figure S1). The correspondence of the first electronic oxidation and reduction waves of

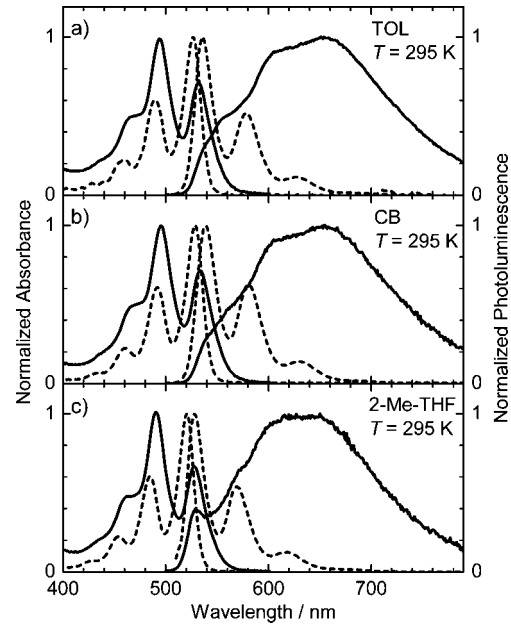

Figure 4. Normalized UV/vis absorption (left axis) and photoluminescence (right axis) spectra of **U-PDI$_2$** (solid lines) and **PDI** (dashed lines) in TOL (a), CB (b), and 2-Me-THF (c) at $T = 295$ K. The excitation wavelength is 495 nm for all emission spectra.

U-PDI$_2$ with those of **PDI** indicates the negligible influence of the xanthene bridge itself on the electronic properties of the dimer.

C. UV/Vis Absorbance at $T = 295$ K. **U-PDI$_2$** is highly soluble and shows concentration-independent absorption spectral shapes, up to at least 10^{-4} M in a wide range of organic solvents. In the concentration range used in this study (10^{-6}−10^{-5} M), it behaves as a purely intramolecular dimer and shows nearly solvent-independent absorption spectra in TOL, chloroform ($CHCl_3$), chlorobenzene (CB), 2-Me-THF, DCM, and *o*-dichlorobenzene (*o*-DCB) (Figure 4 and Supporting Information, Figure S2). Coupling of the parallel transition dipoles of the two stacked PDI moieties leads to delocalization of the excited state and changes the band shape of the absorption spectrum of **U-PDI$_2$** relative to that of **PDI**. Because of a more strongly allowed transition to higher levels, the ground-state absorption of **U-PDI$_2$** shows a blue-shifted absorption maximum and a lower-intensity red-shifted absorption compared to those of **PDI**.[17] The absorption maximum of **U-PDI$_2$** ($\lambda_{max} = 491$−497 nm) is blue shifted by ∼30 nm (0.15 eV) relative to **PDI** ($\lambda_{max} = 521$−531 nm) (Table 1), while the maximum of the lowest-energy peak ($\lambda = 528$−535 nm) in the absorption spectrum of **U-PDI$_2$** is red shifted by ∼5 nm and broadened relative to the lowest-energy absorption peak of **PDI**, such that the absorption onset of **U-PDI$_2$** is red shifted by about 25 nm (0.10 eV) compared to the reference compound in the same solvent.

Hence, the splitting of energy levels caused by dipole−dipole coupling is of similar magnitude as the energy difference between vibronic states of **PDI** (0.16 eV), resulting in a similar energetic position of the 0−1 absorption peak of **PDI** and the maximum of the **U-PDI$_2$** absorption. The weak absorption by the lowest excited state, which is strictly symmetry-forbidden for aligned dipoles, becomes weakly allowed by a nonperfect parallel alignment of the chromophores, which is anticipated from the presence of the orthogonal alkyl chains at the ends of the PDI units which may prevent perfect parallel ordering of the PDI units, and because of the relatively large distance between the chromophores (4.5 Å) in **U-PDI$_2$**.

TABLE 1: Solvent-Dependent Fluorescence Quantum Yields (Φ_F), Fluorescence Decay Time Constants (τ_i), and Corresponding Amplitudes (a_i) at $\lambda_{em} = 650$ nm, Absorption and Emission Maxima (λ_{abs} and λ_{em}), and Singlet Oxygen ($^1\Delta_g$) Luminescence Yields (Φ_Δ) of Air-Equilibrated U-PDI$_2$ Solutions, along with Φ_F of PDI and the Relative Triplet Quantum Yield ($\Phi_{T,rel}$) of Oxygen-Free Solutions of U-PDI$_2$

	PDI		U-PDI$_2$								
solvent	ε_r[a]	Φ_F[b]	Φ_F[b]	a_1	τ_1/ns	a_2	τ_2/ns	λ_{abs}/nm	λ_{em}/nm	Φ_Δ	$\Phi_{T,rel}$[c]
TOL	2.43	1.02	0.17	0.46	0.79	0.54	27.2	494	655	0.22 ± 0.02	1
$CHCl_3$	4.89	1.00	0.15	0.69	1.36	0.31	21.5	497	655	n.d.	n.d.
CB	5.74	0.96	0.13	0.75	1.63	0.25	21.8	496	655	n.d.	n.d.
2-Me-THF	6.97	n.d.[d]	0.06	0.46	1.47	0.54	9.80	491	655	0.57 ± 0.1	2.6
DCM	9.02	n.d.	0.05	0.60	1.78	0.40	9.30	493	(650)[e]	0.43 ± 0.1	2.2
o-DCB	10.36	n.d.	0.02	0.58	1.40	0.42	4.65	493	655	n.d.	n.d.

[a] From ref 28. [b] Measured PL quantum yields (±5%); PDI with 1-hexylheptyl solubilizing groups in DCM was used as a reference ($\Phi_F = 0.99 \pm 0.05$).[29,30] [c] Triplet quantum yield relative to **U-PDI$_2$** in TOL, determined from the photoinduced absorption signal intensity at $\lambda = 570$ nm. [d] n.d.: not determined.[30] [e] There is a higher fluorescence peak at 534 nm in DCM.

D. Steady-State Photoluminescence at $T = 295$ K. Photoexcitation of **U-PDI$_2$** in TOL with an excitation wavelength of $\lambda = 495$ nm leads to PL emission that is heavily changed compared to that of the reference **PDI** (Figure 4a); its emission is broad and strongly red shifted ($\lambda_{max} = 655$ nm) compared to that of **PDI** ($\lambda_{max} = 536$ nm). Additionally, two shoulders (at $\lambda = \sim 550$ and 600 nm) are observed in the PL spectrum. The PL quantum yield amounts to $\Phi_F = 0.17$ and is 6× lower than that of **PDI**, for which $\Phi_F = \sim 1$ (Table 1).

In solvents of higher polarity, taking the relative permittivity (ε_r) as a measure, there are only minor changes to the band shapes of the emission spectra (Figure 4 and Supporting Information, Figure S3). The wavelength of maximal emission intensity remains unchanged in the six different solvents with ε_r in the range of 2.43−10.36 ($\lambda_{max} = 650-655$ nm, Table 1), indicating absence of CT character of the emissive excited state. For the three solvents of highest polarity, additional sharp emission bands (at $\lambda = \sim 530$ and 570 nm) resembling **PDI** emission are resolved, which could be due to a small amount (≤0.6 mol%; see Supporting Information) of a fluorescent impurity. The appearance of this structured emission is actually the consequence of a strong reduction of the PL intensity of the broad emission (Supporting Information, Figure S3) in the order of increasing solvent polarity from TOL ($\varepsilon_r = 2.43$) to $CHCl_3$, CB, 2-Me-THF, DCM, and *o*-DCB ($\varepsilon_r = 10.36$), with $\Phi_F = 0.17$ in TOL reduced to $\Phi_F = 0.02$ in *o*-DCB (Table 1, Figure 5). This indicates the presence of a nonradiative decay channel involving a transition state with CT character.

E. Picosecond Photoinduced Absorption. Possible decay processes of excited states at short time after photoexcitation can be observed by picosecond pump−probe photoinduced absorption spectroscopy (ps-PIA). The ps-PIA spectra of **U-PDI$_2$** in TOL are compared to those of **PDI** in Figure 6. The spectrum of **PDI** shows the bleaching bands ($\lambda = 462$, 490, and 532 nm), the stimulated emission bands ($\lambda = 532$, 582, and 629 nm), and the S_1-S_n absorption ($\lambda = 699$ nm) (Figure 6a, top panel). These signals are decaying with a decay time longer than the instrumentally accessible time window (0−1.8 ns), in correspondence with the PL quantum yield ($\Phi_F = \sim 1$) and the PL lifetime ($\tau = 4.21$ ns) of **PDI** in TOL. For **U-PDI$_2$**, the bleaching band at 490 nm also does not reveal any changes at times shorter than 100 ps, demonstrating the absence of any fast decay to the singlet ground state. The 580 nm transient of **U-PDI$_2$** reveals a rise to positive $\Delta T/T$ that is followed by an ultrafast transition to negative $\Delta T/T$, indicating that stimulated emission is suppressed within 200 fs after photoexcitation. The broad absorption band becomes narrower and blue shifts by 20 nm (from $\lambda_{max} =$ 715 to 695 nm). This leads to rises and decays in the time traces

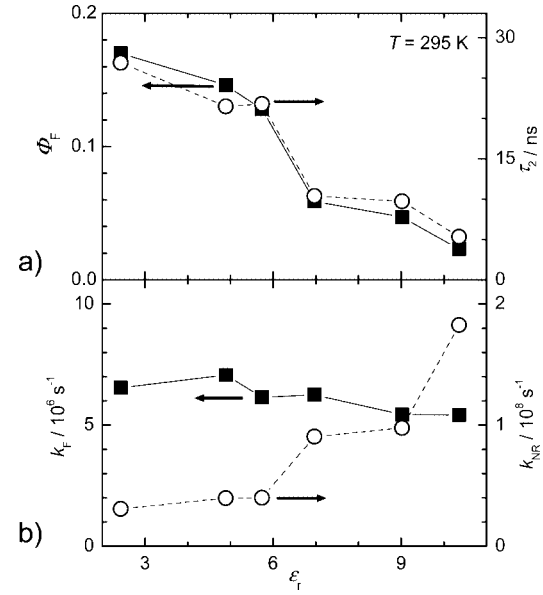

Figure 5. (a) Fluorescence quantum yield (left axis) and the long fluorescence decay component (τ_2) of **U-PDI$_2$** emission at 650 nm (right axis) in various solvents of different polarity at $T = 295$ K. (b) Corresponding radiative (k_F) and nonradiative decay rates (k_{NR}).

at different wavelengths. These spectral changes are attributed to a relaxation of the lowest excited state. Finally, we note that neither the initially created nor the final state of **U-PDI$_2$** is one with fully separated charge carriers because the spectra do not reveal any of the characteristic (sharp) absorptions of the radical cation (at $\lambda = 588$ nm in acetonitrile)[10b] or the radical anion ($\lambda = 700$, 795, 955 nm in acetonitrile or DMF)[10b,31] of the PDI chromophore.

Also in DCM (Supporting Information, Figure S4), the ps-PIA spectra of **U-PDI$_2$** do not show any changes in the intensity of the bleaching, confirming the absence of fast decay to the ground state at these short time delays (up to 200 ps). The absorption shows a spectral shift in the wavelength interval of 550−800 nm and a narrowing in about 200 ps but again does not reveal the formation of radical ions. Also, using NIR detection (900−1150 nm), the ps-PIA spectra do not reveal radical anions of **PDI** but only S_1-S_n absorption.

F. Time-Resolved Fluorescence at $T = 295$ K. Time-resolved fluorescence (TR-PL) measurements were carried out in the (sub-)nanosecond time range in order to further characterize the spectral shape of the **U-PDI$_2$** PL emission and to analyze the solvent dependence of the fluorescence in more detail. Upon photoexcitation with $\lambda = 400$ nm, the time-resolved emission spectra of **U-PDI$_2$** in TOL (Figure 7a) show that after a ∼10

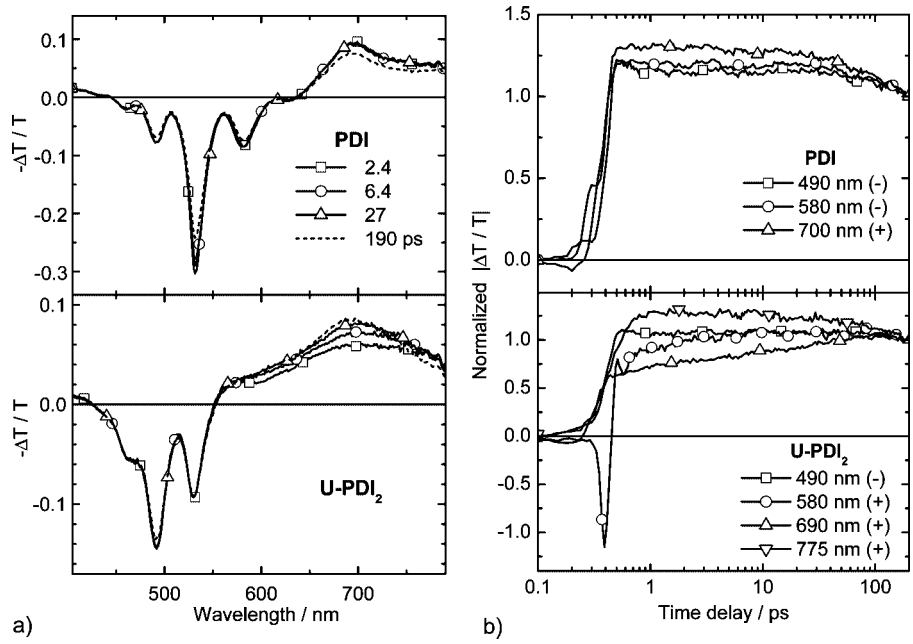

Figure 6. ps-PIA spectra (a) and decay traces (b) of **PDI** (top) and **U-PDI$_2$** (bottom) in TOL at $T = 295$ K and at time delays of 0−200 ps ($\lambda_{exc} = 530$ nm). The decay traces are normalized to 1 at a time delay of 200 ps. The sign in parentheses indicates the sign of the $-\Delta T/T$ signal at 200 ps, prior to normalization, that is, "(+)" indicates reduced transmission.

ns delay, the emission decays monoexponentially over the full spectral window with a PL maximum (665 nm) and shoulders (∼550 and 600 nm) in perfect correspondence with the steady-state PL spectrum (Figure 4a). The time-integrated contribution of this long decay component ($\tau_2 = 27.2$ ns, vide infra) amounts to ∼90% of the total emission in the wavelength interval of 520−700 nm (Figure 7b). We will show in the next section that this long-lived emission involves decay from an equilibrium of two excited states.

Analysis of TR-PL traces (Figure 7c) at $\lambda_{em} = 650$ nm in terms of a sum of two exponential decays yields a good fit to the data, indicating the involvement of at least two excited states in the luminescence.[32] The short-lived component ($\tau_1 = 0.79$ ns with amplitude $a_1 = 0.46$) is shorter than the decay time of **PDI** ($\tau = 4.21$ ns), while the long-lived component—the main contribution—has a much longer decay component ($\tau_2 = 27.2$ ns, $a_2 = 0.54$). At $\lambda = 540$ nm, an additional intermediate decay time of $\tau_3 = \sim 4$ ns must be added to give a proper fit to the data, which could originate from a fluorescent impurity. In the five other solvents (Supporting Information, Figure S5), the TR-PL traces also reveal a short ($\tau_1 = \sim 1.5$ ns with $a_1 = \sim 0.6$) and a long ($\tau_2 = 5.65-24.8$ ns with $a_2 = \sim 0.4$) decay component at $\lambda = 650$ nm (Table 1). Notably, the lifetime of the long decay component decreases with increasing ε_r of the solvent (Figure 5), along with the reduction of the PL quantum yield. This shows that the PL quenching at higher ε_r is caused by a faster nonradiative decay of the long-lived (equilibrium of) excited state(s) and not by quenching of a precursor of that state. This is in correspondence with the absence of fast decay of the bleaching band in the ps-PIA experiments. The rates of the radiative (k_F) and nonradiative (k_{NR}) decay channel from the (equilibrium of) excited state(s) can be determined from Φ_F and τ_2, neglecting the short decay components, by using $k_{NR} = (1 - \Phi_F)/\tau_2$ and $k_F = 1/\tau_2 - k_{NR}$. From this, we find a nearly constant $k_F = 5-7 \times 10^6$ s^{-1}, while k_{NR} is faster and increases with a factor of 6, from 3.1×10^7 s^{-1} in TOL to 18×10^7 s^{-1} in *o*-DCB (Figure 5b).[33]

In summary, the TR-PL data analysis shows that, irrespective of the solvent used, the **U-PDI$_2$** emission is characterized by two decay times, revealing the involvement of at least two excited states. The longer-lived component amounts to ∼90% of the total emission in TOL and reveals a broad emission spectrum with a maximum at ∼660 nm and shoulders at 555 and 600 nm. From the combined steady-state and time-resolved PL, we find that in more polar solvents, the excited state(s) decay faster via a nonradiative decay channel ($k_{NR} = 3-18 \times 10^7$ s^{-1}). Further, the (equilibrium of) excited state(s) has a long intrinsic decay time of $\tau_F = k_F^{-1} = \sim 200$ ns.

G. Temperature Dependence of Fluorescence. We will use the spectral shape of **U-PDI$_2$** fluorescence and its PL yields and decay times as complementary tools to find information on the relaxation processes of photoexcited **U-PDI$_2$** in TOL and 2-Me-THF by temperature-dependent studies.

T well below T_m^{SOL}. At temperatures well below the melting points of the solvents ($T_m^{TOL} = 180$ K and $T_m^{2\text{-Me-THF}} = 137$ K), the PL characteristics of **U-PDI$_2$** substantially differ from those at $T = 295$ K. First, in both solvents, the PL quantum yields are much higher; $\Phi_F = \sim 0.6$ in both solvents at the lowest temperatures, which is ∼4 and 10× higher than those at 295 K for TOL and 2-Me-THF, respectively (Figure 8a−d). Second, the PL decay at 650 nm is much slower at low temperature and is characterized by two decay times, $\tau_1 = 14.2$ and 43.8 ns ($a_1/a_2 = 1.03$) in TOL at 135 K and $\tau = 14.2$ and 48.2 ns ($a_1/a_2 = 1.05$) in 2-Me-THF at 80−100 K. Third, the spectral shapes show significant changes with respect to those at 295 K; in a glassy matrix of TOL ($T = 135$ K), the spectrum is blue shifted ($\lambda_{max} = 614$ nm) and shows a distinct vibronic progression. Also, in glassy 2-Me-THF (for example, at $T = 100$ K), the steady-state emission (Figure 8b) is strongly blue shifted, and a similarly structured emission is revealed in a time-resolved emission spectrum (Figure 8e), taken at a delay of 30−35 ns after photoexcitation.

Thus, at temperatures well below the melting points of the solvents, **U-PDI$_2$** reveals much more intense and longer-lived

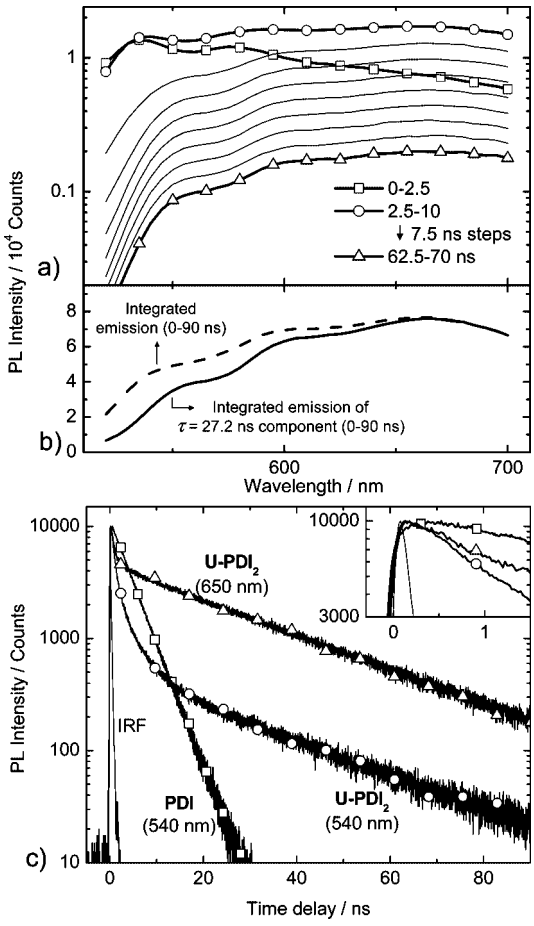

Figure 7. Fluorescence decay of **U-PDI$_2$** in TOL at $T = 295$ K upon excitation with $\lambda_{exc} = 400$ nm. (a) Time-resolved emission spectra at the indicated time windows. For the first time window, the width is 2.5 ns, while it is 7.5 ns at longer delay times. (b) Time-integrated PL spectra (at 0−90 ns time delay) for all emission (dashed line) and for the emission having a 27.2 ns decay time (solid line). (c) Decay traces of **U-PDI$_2$** at $\lambda = 540$ and 650 nm, compared to that of **PDI** in TOL ($\lambda = 540$ nm). The inset of (c) shows the decay at short time delay, and the thin line indicates the instrumental response function (IRF).

emission than at 295 K. The emission is vibronically resolved, and its 0−0 transition matches with the onset of the corresponding absorption spectrum. The high quantum yields and the long lifetime indicate that nonradiative decay channels are prevented under these conditions. This emission is assigned to the lowest singlet exciton state (LE).

T approaching T_m^{SOL}. Warming of TOL (between 135 and $T_m = 180$ K) and 2-Me-THF (between 110 and $T_m = 137$ K) invokes strong reductions of the PL decay time and the PL intensity (Figure 8a−d). Starting from ∼40 K below T_m, the short PL decay component is strongly reduced with increasing temperature, from $\tau_1 = 15$ ns at low temperature to ∼2 ns at T_m. Additionally, its intensity relative to that of the longer component (a_1/a_2) strongly increases in this temperature range. Thus a nonradiative decay channel becomes active at higher temperature. Simultaneously, a red shift of the emission and a loss of vibronic structure are observed, revealing that a different excited state is populated, which is prevented below T_m. The excited state is assigned to an excimer-like state (E).

T above T_m^{SOL}. In TOL (and CB, Supporting Information, Figure S6), the PL yield slightly increases with increasing temperature above $T = \sim 200$ K. Simultaneously, the spectra shift to higher energy, and vibronic features appear at $T \geq 290$ K, at ∼550 nm and 600 nm in both solvents (Figure 9a and Supporting Information). This demonstrates that at higher temperature, the LE state is repopulated from the E state. The increasing PL yield indicates that the LE is more emissive than the E excited state. At the highest temperatures, the PL spectrum again shows vibronic features at the high-energy side close to the onset of absorption. The low-temperature (120 K) spectrum is 20 nm red shifted from the LE spectrum at 370 K, in correspondence with a similar red shift of the low-energy absorption band.

In TOL, E-type emission is most prominent at 175 K, next to some residual short-lived emission at higher energy, while LE-type emission is virtually absent. At 370 K, the emission is dominated by LE emission, but some E-type emission may still be overlapping. The characteristic E-type and LE-type emission spectra at these temperatures are shown in Figure 9b, with the LE emission corrected for some E-type emission. These spectra were used to find the relative PL quantum yields (Φ_E/Φ_{LE}) of the two types of emission as a function of reciprocal temperature (Figure 10). This can be used to estimate the activation energy to form the LE from the E state (E_a) at the low-temperature limit and the energy difference between the two states (ΔH) at the high-temperature limit (Figure 2). The slopes of Φ_E/Φ_{LE} versus $1/T$ are equal to[34]

$$\frac{d\left(\log\frac{\Phi_E}{\Phi_{LE}}\right)}{d(1/T)} = \log(e)\frac{\Delta H}{k_B} \qquad \text{at the high-temperature limit} \qquad (1)$$

and

$$\frac{d\left(\log\frac{\Phi_E}{\Phi_{LE}}\right)}{d(1/T)} = -\log(e)\frac{E_a}{k_B} \qquad \text{at the low-temperature limit} \qquad (2)$$

under the assumptions that the radiative decay rates of the E and LE states are independent of temperature. At the high-temperature limit, we find that the LE state is higher in energy than the E state by $\Delta H = 0.22$ eV, in close correspondence with the observed red shift of the onset of E-type emission relative to that of LE-type emission (0.23 eV, Figure 9b).[35,36] From the low-temperature limit, we estimate $E_a = 0.24$ eV for the barrier between the E state and the LE state (Figure 2).

For 2-Me-THF, the PL spectra also shift to higher energy with increasing temperature, and some vibronics (at ∼550 and 600 nm) are superimposed on the PL spectrum at $T = 295$ K (Figure 8b and e). Thus, also in 2-Me-THF, the LE state can be repopulated from the E state at higher temperature. Remarkably, opposite to the results in TOL, above $T = 200$ K, the PL yield and the PL decay time continue to drop with increasing temperature (Figure 8d), indicating the presence of an additional temperature-activated nonradiative deactivation pathway of the equilibrated excited state in 2-Me-THF that is not apparent in TOL.

H. Triplet State Population via the CT Transition State. At longer times after photoexcitation, triplet excited states of **U-PDI$_2$** are populated in TOL at $T = 295$ K. The near-steady-state PIA (ss-PIA) spectrum with a modulation frequency of 275 Hz reveals that the S_1-S_n absorption band at 690 nm is replaced by a characteristic PDI T_1-T_n absorption in the same spectral region as the bleaching bands (Figure 11a).[10a] As a check, *N*-methylfulleropyrrolidine (MP-C$_{60}$) with a triplet energy of $E(T_1) = \sim 1.50$ eV[37] was codissolved with **PDI** ($E(T_1) = \sim 1.20$ eV)[10] and photoexcited, rendering a very similar PDI T_1-T_n absorption spectrum via triplet energy transfer from MP-C$_{60}$ to **PDI** (Figure 11b). In **U-PDI$_2$**, the triplet states must be populated in the time scale between 0.86 and 150 ns, that is,

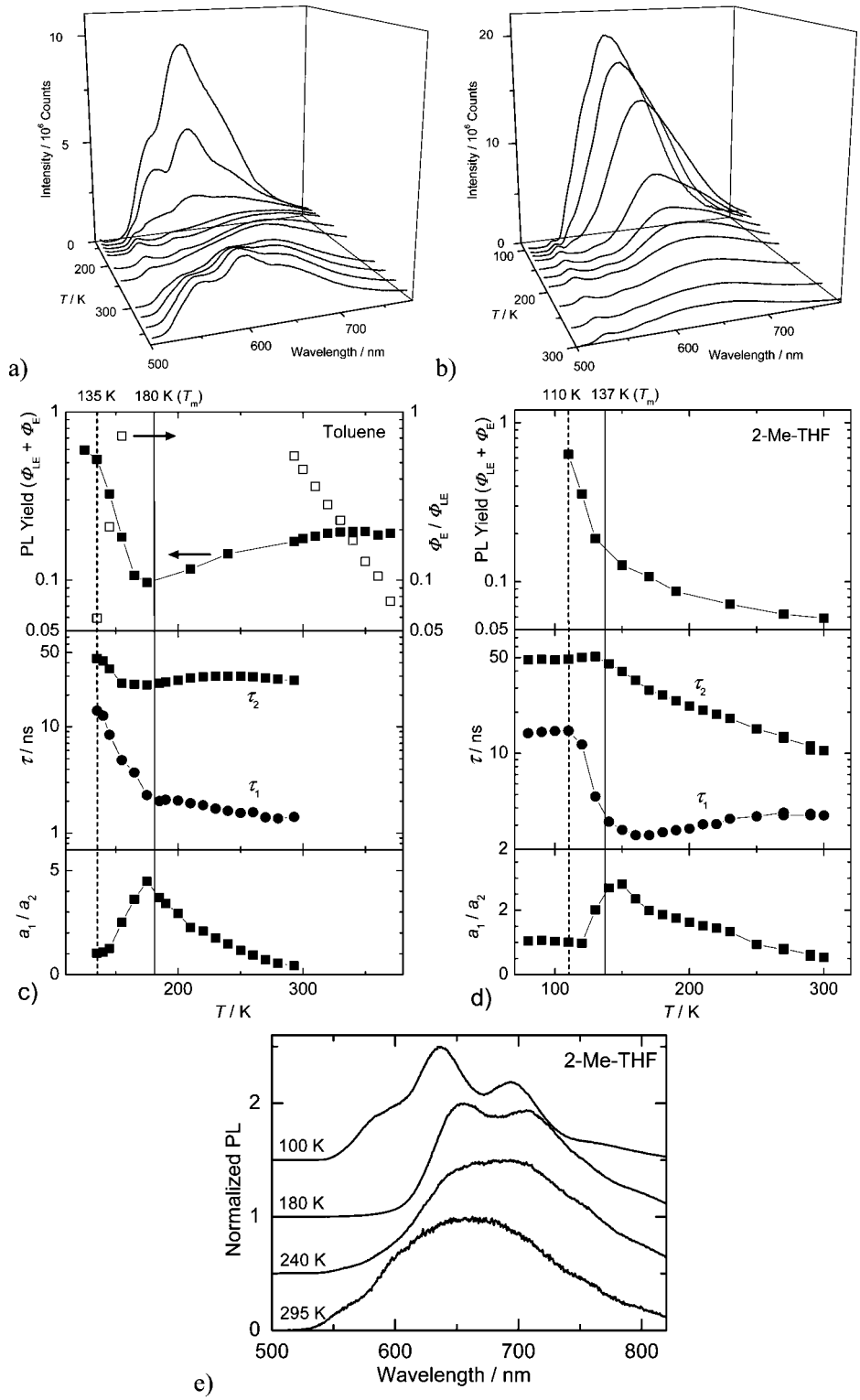

Figure 8. (a,b) Temperature-dependent steady-state PL spectra of **U-PDI$_2$** in TOL and 2-Me-THF. (c,d) Temperature-dependent PL yields of **U-PDI$_2$** in TOL (±20%) and 2-Me-THF (±10%) and results of TR-PL analyses. The vertical solid lines indicate the melting points of the solvents, and the dashed lines are a guide to the eye. The open symbols in (c) indicates Φ_E/Φ_{LE} as determined from analysis of steady-state PL spectra. (e) Time-resolved emission spectra of **U-PDI$_2$** in 2-Me-THF, at the indicated temperatures, and a 30−35 ns delay after photoexcitation with $\lambda = 488$ nm. These spectra are offset for clarity.

between the end of the ps-PIA time scale at which no T_1-T_n absorption was observed and the first nanosecond PIA (ns-PIA) spectrum that we were able to obtain (Figure 11b) and after which the signal intensity decayed. Thus, although we were unable to visualize the direct conversion from the S_1-S_n to the T_1-T_n absorption of **U-PDI$_2$**, the growth rate of the T_1-T_n absorption band can comply with the decay time ($\tau_2 = 27.2$ ns) of the long-lived **U-PDI$_2$** emission, indicating that the triplet excited state could be formed from the emissive excited state. The lifetime of the triplet excited state is $\tau_T = 200 \pm 50$ μs in oxygen-free TOL, in correspondence with the lifetime of monomeric PDI.[10] Upon addition of oxygen, the triplet state of **U-PDI$_2$** is quantitatively quenched, in accord with an $E(T_1)$ higher than the energy of singlet oxygen ($^1\Delta_g$) above its triplet

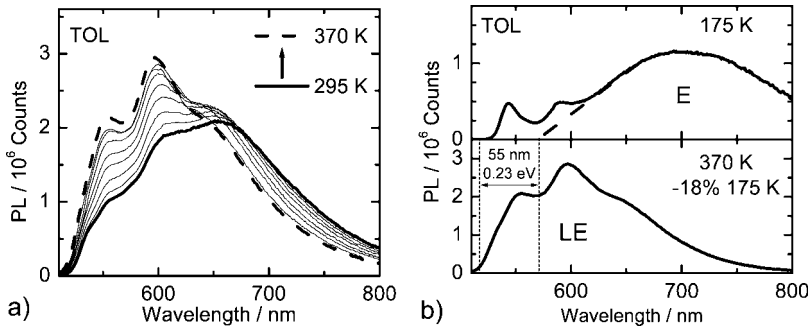

Figure 9. (a) Temperature-dependent photoluminescence of **U-PDI$_2$** in TOL upon excitation with $\lambda = 495$ nm. (b) PL spectra showing the contributions of the E-type and LE-type emissions.

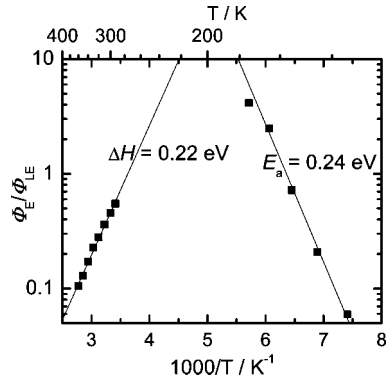

Figure 10. The temperature-dependent relative PL quantum yields (Φ_E/Φ_{LE}) of **U-PDI$_2$** in TOL and the energies derived from these.

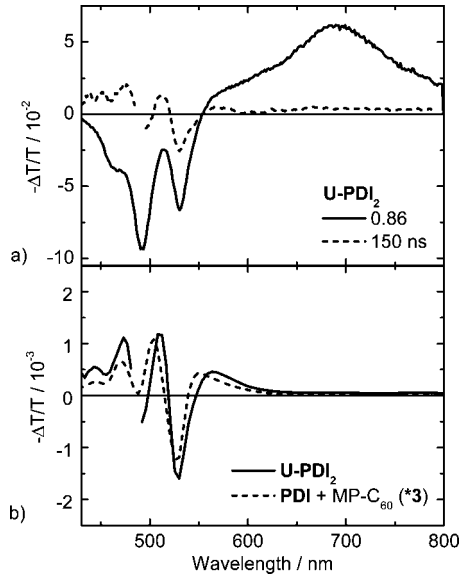

Figure 11. (a) PIA spectra of **U-PDI$_2$** in TOL at $T = 295$ K using $\lambda_{exc} = 490$ nm at 0.86 ns (air-saturated) and a 150 ns (oxygen-free) delay after photoexcitation. (b) Near-steady-state photoinduced absorption spectra of **PDI** and MP-C$_{60}$ (1:1, $\lambda_{exc} = 351 + 364$ nm) and **U-PDI$_2$** ($\lambda_{exc} = 488$ nm) in oxygen-free TOL at $T = 295$ K and using a modulation frequency of 275 Hz.

ground state (0.98 eV). We predict that $E(T_1)$ of **U-PDI$_2$** is similar to that of monomeric perylenediimides, for which $E(T_1) = \sim 1.20$ eV.[10]

The relative triplet quantum yields $\Phi_{T,rel}$ of **U-PDI$_2$** in oxygen-free solutions were determined from the T_1-T_n absorption intensity at 570 nm, where ground-state bleaching is absent (Table 1, Supporting Information, Figure S7). In the more polar solvents DCM and 2-Me-THF, we found T_1-T_n absorption intensities that were 2.6 and 2.2× higher than that in TOL,

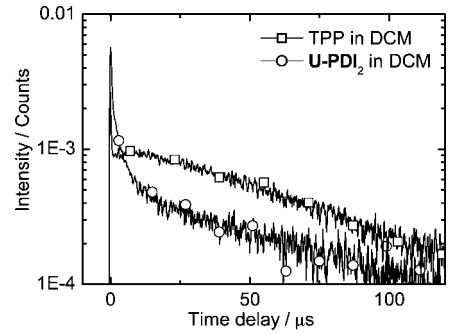

Figure 12. Singlet oxygen ($^1\Delta_g$) luminescence decay traces at a laser fluence of 4.9 J m^{-2} for TPP and **U-PDI$_2$** in DCM ($\lambda_{exc} = 532$ nm, $\lambda_{em} = 1270$ nm).

respectively. At $T = 200$ K in DCM, the amount of triplet absorption reduces by about 40% with respect to 295 K. Thus, in more polar solvents and at higher temperature, more triplets are formed, indicating a temperature-activated process via a CT transition state or a high-energy-intermediate CT state. Our experiments cannot distinguish between these two possibilities, and the precise nature of this state is uncertain. In the following, we denote this state as the CT transition state.

I. Singlet Oxygen Luminescence. Singlet oxygen ($^1\Delta_g$) quantum yields (Φ_Δ) were determined for **U-PDI$_2$** in benzene, TOL, 2-Me-THF, and DCM by photoexcitation at 532 nm and probing the oxygen ($^1\Delta_g$) phosphorescence decay with time using:[38,39]

$$\Phi_\Delta = \frac{n^2 I_P^0 k_P(\mathrm{ST})}{n^2(\mathrm{ST}) I_P^0(\mathrm{ST}) k_P} \Phi_\Delta(\mathrm{ST}) \qquad (3)$$

with n as the refractive index of the solvent,[28] I_P^0 as the extrapolated phosphorescence intensity at $t = 0$, and k_P as the rate of radiative decay from the singlet oxygen ($^1\Delta_g$) state, taken from Scurlock et al., who reported k_P relative to that in benzene ($k_P' = k_P/k_P(\mathrm{benzene})$).[39] ST denotes standard, here, C$_{60}$ in benzene with $\Phi_\Delta = 0.95 \pm 0.05$.[40,41] The singlet oxygen yields were checked with TPP (*meso*-tetraphenylporphyrin), for which we determined $\Phi_\Delta = 0.70$ in benzene, 2-Me-THF, as well as DCM and $\Phi_\Delta = 0.60$ in TOL, in good correspondence with previously determined values.[38,42] The laser power dependence was carefully checked in each experiment, and we found that only at laser fluences above 6.0 J m^{-2} did the signal intensity start to deviate from linearity.[43] Figure 12 shows two luminescence decay traces at 1270 nm. At early times (< 20 μs), the traces of the TPP and notably of the **U-PDI$_2$** solution reveal additional short components that are absent in the C$_{60}$ trace, which reveals only a rise of the oxygen ($^1\Delta_g$) luminescence. These short components are probably caused by saturation of

TABLE 2: Solvent-Dependent Fluorescence Quantum Yields (Φ_F), Singlet Oxygen ($^1\Delta_g$) Luminescence Yields (Φ_Δ) of Air-Equilibrated U-PDI$_2$ Solutions, the Triplet Quantum Yields (Φ_T), and Rate Constants Derived from These

solvent	Φ_F	Φ_Δ	Φ_T[a]	$k_F/10^6$ s^{-1}	$k_{NR}/10^6$ s^{-1}	$k_{ISC}/10^6$ s^{-1}[b]	$k_{NR,G}/10^6$ s^{-1}[b]
TOL	0.17	0.22 ± 0.02	0.20−0.36	6.5	31	7.5−13 (8.2)	18−24 (23)
2-Me-THF	0.06	0.57 ± 0.1	0.47−0.94	6.3	90	45−90 (55)	0−45 (35)
DCM	0.05	0.43 ± 0.1	0.40−0.80	5.4	98	41−83 (44)	15−57 (54)

[a] The lower limits are obtained from $\Phi_T \geq \Phi_\Delta$ and the upper limits from ns-PIA results and $\Phi_F^{2\text{-Me-THF}}$ (see text). The lower limit for Φ_T^{DCM} results from the lower limit for $\Phi_T^{2\text{-Me-THF}}$ and the ns-PIA data ($\Phi_T^{DCM} = 0.85 \times \Phi_T^{2\text{-Me-THF}}$). [b] The values in parentheses are those when using the average value of Φ_Δ as a measure for Φ_T, assuming $f_T \times S_\Delta = 1$.

the detector by residual photoluminescence, extending into the near infrared.[44,45] After a ~20 μs delay, the signal intensity decays with a similar rate constant, and these decays were used to determine Φ_Δ. For **U-PDI$_2$**, Φ_Δ decreases in the order 2-Me-THF ($\Phi_\Delta = 0.57$), DCM ($\Phi_\Delta = 0.43$), TOL ($\Phi_\Delta = 0.22$), and benzene ($\Phi_\Delta = 0.22$), in perfect correspondence with the relative T_1-T_n absorption intensities in oxygen-free solutions measured with ns-PIA (Table 1).

Using the relation $\Phi_\Delta = \Phi_T \times f_T$ (the fraction of triplet states scavenged by oxygen in a given system) $\times S_\Delta$ (the efficiency of singlet oxygen ($^1\Delta_g$) generation from the quenched triplet state), Φ_Δ gives a lower limit for the triplet quantum yield (Φ_T) of **U-PDI$_2$**. The relative triplet quantum yields obtained by ns-PIA ($\Phi_T^{DCM} = 0.85 \times \Phi_T^{2\text{-Me-THF}}$ and $\Phi_T^{TOL} = 0.38 \times \Phi_T^{2\text{-Me-THF}}$, Table 1) provide upper limits for Φ_T^{DCM} and Φ_T^{TOL}, while $\Phi_T^{2\text{-Me-THF}} < 0.94$ because $\Phi_F^{2\text{-Me-THF}} = 0.06$. Using Φ_F and Φ_T and the total nonradiative decay rate ($k_{NR} = k_{ISC} + k_{NR,G}$, where $k_{NR,G}$ expresses the nonradiative decay directly to the ground state) obtained in subsection F, the ISC rates (k_{ISC}) and $k_{NR,G}$ can be obtained using

$$k_{ISC} = \frac{\Phi_T}{1-\Phi_F} k_{NR} \quad (4)$$

$$k_{NR,G} = \frac{1-\Phi_T-\Phi_F}{1-\Phi_F} k_{NR} \quad (5)$$

The results are summarized in Table 2 for **U-PDI$_2$** in TOL, 2-Me-THF, and DCM. We find that k_{ISC} is faster by 3−12× in more polar solvents than TOL; in 2-Me-THF and DCM, $k_{ISC} = 40-90 \times 10^6$ s^{-1}, while in TOL, it is $7-13 \times 10^6$ s^{-1}. The differences in the k_{ISC} between 2-Me-THF and DCM and in $k_{NR,G}$ for the three solvents are smaller than the experimental error.

Discussion

The results of the deactivation of excited states for **U-PDI$_2$** in TOL and 2-Me-THF are summarized with a schematic diagram (Figure 2). In TOL, we find that the LE state is higher in energy than the E state by $\Delta H = 0.22$ eV, and we find $E_a = 0.24$ eV as the activation barrier between the LE state and the E state. At $T = 295$ K, an equilibrium between the two states is present in both solvents. Because of the absence of solvatochromism and of radical ions in the PIA spectra, we conclude that the E state has negligible CT character. Hence, we suggest that ΔH and E_a are similar for **U-PDI$_2$** in the more polar solvent 2-Me-THF. The main difference between the two solvents is that for 2-Me-THF, an additional temperature-activated nonradiative process is active. Solvent-dependent PL yields and lifetimes reveal that this deactivation occurs via a CT transition state, populating, in addition to the singlet ground state, the lowest triplet excited state much more efficient than that in monomeric PDI. Once formed, the triplet excited state of **U-PDI$_2$** shows similar characteristics (triplet lifetime, T_1-T_n absorption spectrum) as those of monomeric PDI, indicating a localized nature of the state.

The mechanism of ISC from the CT transition state to the triplet excited state is not apparent from the measurements, and more detailed studies will be necessary to resolve this issue. However, we note that the radical pair intersystem crossing (RP-ISC) mechanism in which ISC (^{1}CT → ^{3}CT) is followed by a rapid spin-allowed charge recombination (^{3}CT → T_1) requires weak electronic coupling between the donor and the acceptor unit to allow a spin flip in the CT state. Oppositely, the spin−orbit intersystem crossing (SO-ISC) mechanism in which charge recombination (^{1}CT → T_1) is accompanied by a simultaneous change in spin−orbit momentum is favored by strong electronic coupling between the radical ions. In **U-PDI$_2$**, the close proximity (~4.5 Å, or less) and parallel alignment of the PDI units allow for strong coupling between the radical ions, and the SO-ISC mechanism is, in our view, the most probable candidate to explain the enhanced ISC in the dimer relative to monomeric PDI.

It is of interest to have a further look at the solvent dependence of the nonradiative decay rates, k_{ISC} and $k_{NR,G}$, that is, intersystem crossing and direct decay to the ground state from the LE and E states. If Φ_Δ is taken as a lower limit for Φ_T, most differences in k_{ISC} and $k_{NR,G}$ are smaller than the experimental error for the three solvents used (TOL, 2-Me-THF, and DCM). However, we note that f_T is probably very close to unity because the long triplet lifetime of **U-PDI$_2$** enables efficient triplet quenching by O_2. Also, S_Δ of $\pi-\pi^*$-excited triplet states of aromatic hydrocarbons is generally close to unity ($S_\Delta = 0.8-1.0$).[46] Hence, by assuming $f_T \times S_\Delta = 1$, we find a distinct increase of $k_{NR,G}$ from 23×10^6 s^{-1} in TOL to 35×10^6 s^{-1} in 2-Me-THF and 54×10^6 s^{-1} in DCM (Table 2). Using the same approximation for k_{ISC}, we obtain 8×10^6 s^{-1} in TOL, 55×10^6 s^{-1} in 2-Me-THF, and 44×10^6 s^{-1} in DCM (Table 2); this is more than an order of magnitude faster than k_{ISC} in monomeric PDI for which values of $<10^6$ s^{-1} have been reported.[10] The increase of k_{ISC} in more polar environments is a consequence of a lowering of the CT transition state under these conditions. This causes the increased conversion of LE/E into T (Figure 2). The fact that $k_{NR,G}$ also increases shows that the CT transition state is also involved in the conversion of LE/E into the S_0 ground state.

Conclusions

We have used a cofacially stacked PDI dimer **U-PDI$_2$** as a molecular model to study the enhanced population of triplet excited states via CT states. Such enhanced triplet formation has recently been identified in electron donor−acceptor polymer blends and may limit the performance of future organic photovoltaic devices.[1] Figure 2 describes the formation and decay processes of the various singlet and triplet excited states of **U-PDI$_2$** following photoexcitation. The starting point is the

vibrationally relaxed lowest singlet exciton state (LE) formed by photoexcitation that structurally resembles the ground state.

At low temperatures, where the conformation of the LE state is "frozen", the PL spectrum of **U-PDI$_2$** exhibits vibronic structure with only a small Stokes shift for the 0−0 transitions. Due to exciton coupling in the stacked system, decay from the LE state is symmetry-forbidden, and hence, the PL decay time is long. At intermediate temperatures, conformational relaxation of the LE state leads to the formation of an intramolecular excimer (E) state in **U-PDI$_2$**, likely having a reduced distance between the two PDI units, enabling stronger delocalization of π-electrons. The E-type emission of **U-PDI$_2$** is unstructured, broad, and red shifted compared to LE emission. The large Stokes shift, typical large for excimers, is consistent with conformational changes in the E state. Solvatochromic shifts of the E emission are negligible, indicating that the E state has minimal CT character.[22] Although photoinduced electron transfer does not occur in **U-PDI$_2$** because lower-energy CT states are unavailable, the stacking of PDI chromophores creates a CT transition or intermediate state ($PDI^{\bullet+}-PDI^{\bullet-}$) at energies just above the emissive singlet states. Photoinduced absorption measurements and singlet oxygen ($^1\Delta_g$) luminescence measurements demonstrate that intersystem crossing is enhanced by the presence of this CT transition state and occurs much faster and more efficient in solvents of higher polarity, where CT states are lowered in energy. As a consequence, the quantum yield for triplet formation in cofacially stacked PDI dimers can be orders of magnitude higher than that of monomeric PDI chromophores.

The high quantum yields for triplet formation (estimated to be more than 50%) in these cofacially stacked chromophores and the role of a polar CT transition state gives strong reason to assume that intersystem crossing via CT states can represent a major loss mechanism in organic photovoltaic cells. This calls for further investigation as well as for design of materials or architectures that avoid it.

Acknowledgment. This work was supported by the EU Integrated Project NAIMO (No NMP4-CT-2004−500355).

Supporting Information Available: Experimental details, including electrochemistry, solvent-dependent UV/vis absorption and photoluminescence, and photoinduced absorption spectra. This information is available free of charge via the Internet at http://pubs.acs.org.

References and Notes

(1) (a) Ford, T. A.; Avilov, I.; Beljonne, D.; Greenham, N. C. *Phys. Rev. B* **2005**, *71*, 125212. (b) Offermans, T.; van Hal, P. A.; Meskers, S. C. J.; Koetse, M. M.; Janssen, R. A. J. *Phys. Rev. B* **2005**, *72*, 045213. (c) Veldman, D.; Offermans, T.; Sweelssen, J.; Koetse, M. M.; Meskers, S. C. J.; Janssen, R. A. J. *Thin Solid Films* **2006**, *511−512*, 333. (d) Ohkita, H.; Cook, S.; Astuti, Y.; Duffy, W.; Heeney, M.; Tierney, S.; McCulloch, I.; Bradley, D. D. C.; Durrant, J. R. *Chem. Commun.* **2006**, 3939. (e) Veldman, D.; Ipek, Ö.; Meskers, S. C. J.; Sweelssen, J.; Koetse, M. M.; Veenstra, S. C.; Kroon, J. M.; van Bavel, S. S.; Loos, J.; Janssen, R. A. J. *J. Am. Chem. Soc.* doi 10.1021/ja8012598.

(2) Turro, N. J. *Modern Molecular Photochemistry*; University Science Books: New York, 1991.

(3) van Willigen, H.; Jones, G.; Farahat, M. S. *J. Phys. Chem.* **1996**, *100*, 3312.

(4) Wiederrecht, G. P.; Svec, W. A.; Wasielewski, M. R.; Galili, T.; Levanon, H. *J. Am. Chem. Soc.* **2000**, *122*, 9715.

(5) (a) Dutton, P. L.; Leigh, J. S.; Seibert, M. *Biochem. Biophys. Res. Commun.* **1972**, *46*, 406. (b) Thurnauer, M. C.; Katz, J. J.; Norris, J. R. *Proc. Natl. Acad. Sci. U.S.A.* **1975**, *72*, 3270. (c) Levanon, H.; Norris, J. R. *Chem. Rev.* **1978**, *78*, 185.

(6) (a) Hasharoni, K.; Levanon, H.; Greenfield, S. R.; Gosztola, D. J.; Svec, W. A.; Wasielewski, M. R. *J. Am. Chem. Soc.* **1995**, *117*, 8055. (b) Carbonera, D.; DiValentin, N.; Corvaja, C.; Agostini, G.; Giacometti, G.; Liddell, P. A.; Kuciauskas, D.; Moore, A. L.; Moore, T. A.; Gust, D. *J. Am. Chem. Soc.* **1998**, *120*, 4398.

(7) Okada, T.; Karaki, I.; Matsuzawa, E.; Mataga, N.; Sakata, Y.; Misumi, S. *J. Phys. Chem.* **1981**, *85*, 3957.

(8) Dance, Z. E. X.; Mi, Q.; McCamant, D. W.; Ahrens, M. J.; Ratner, M. A.; Wasielewski, M. R. *J. Phys. Chem. B* **2006**, *110*, 25163.

(9) Langhals, H. *Helv. Chim. Acta* **2005**, *88*, 1309.

(10) (a) Ford, W. E.; Kamat, P. V. *J. Phys. Chem.* **1987**, *91*, 6373. (b) Kircher, T.; Löhmannsröben, H.-G. *Phys. Chem. Chem. Phys.* **1999**, *1*, 3987.

(11) (a) Baffreau, J.; Leroy-Lhez, S.; Vân Anh, N.; Williams, R. M.; Hudhomme, P. *Chem.—Eur. J.* **2008**, in press. (b) Prodi, A.; Chiorboli, C.; Scandola, F.; Iengo, E.; Alessio, E.; Dobrawa, R.; Würthner, F. *J. Am. Chem. Soc.* **2005**, *127*, 1454. (c) Ghirotti, M.; Chiorboli, C.; You, C.-C.; Würthner, F.; Scandola, F. *J. Phys. Chem. A* **2008**, *112*, 3376.

(12) (a) Würthner, F.; Thalacker, C.; Sautter, A.; Schartel, W.; Ibach, W.; Hollricher, O. *Chem.—Eur. J.* **2000**, *6*, 3871. (b) Würthner, F.; Thalacker, C.; Diele, S.; Tschierske, C. *Chem.—Eur. J.* **2001**, *7*, 2245. (c) Syamakumari, A.; Schenning, A. P. H. J.; Meijer, E. W. *Chem.—Eur. J.* **2002**, *8*, 3353. (d) Wang, W.; Li, L.-S.; Helms, G.; Zhou, H.-H.; Li, A. D. Q. *J. Am. Chem. Soc.* **2003**, *125*, 1120. (e) Wang, W.; Wan, W.; Zhou, H.-H.; Niu, S.; Li, A. D. Q. *J. Am. Chem. Soc.* **2003**, *125*, 5248. (f) Würthner, F.; Chen, Z.; Dehm, V.; Stepanenko, V. *Chem. Commun.* **2006**, 1188. (g) Chen, Z.; Stepanenko, V.; Dehm, V.; Prins, P.; Siebbeles, L. D. A.; Seibt, J.; Marquetand, P.; Engel, V.; Würthner, F. *Chem.—Eur. J.* **2007**, *13*, 436.

(13) (a) Forrest, S. R. *Chem. Rev.* **1993**, *97*, 1793. (b) Gómez, U.; Leonhardy, M.; Port, H.; Wolf, H. C. *Chem. Phys. Lett.* **1997**, *268*, 1. (c) Soos, Z. G.; Hennessy, M. H.; Wen, G. *Chem. Phys.* **1998**, *227*, 13. (d) Hennessy, M. H.; Soos, Z. G., Jr.; Girlando, A. *Chem. Phys.* **1999**, *245*, 199. (e) Hoffmann, M.; Schmidt, K.; Fritz, T.; Hasche, T.; Agranovich, V. M.; Leo, K. *Chem. Phys.* **2000**, *258*, 73. (f) Kobitski, A. Yu.; Scholz, R.; Vragoviæ, I.; Wagner, H. P.; Zahn, D. R. T. *Phys. Rev. B* **2002**, *66*, 153204. (g) Kobitski, A. Yu.; Scholz, R.; Zahn, D. R. T.; Wagner, H. P. *Phys. Rev. B* **2003**, *68*, 155201. (h) Vragoviæ, I.; Scholz, R. *Phys. Rev. B* **2003**, *68*, 155202. (i) Scholz, R.; Kobitski, A. Yu.; Vragoviæ, I.; Wagner, H. P.; Zahn, D. R. T. *Org. Electron.* **2004**, *5*, 99. (j) Scholz, R.; Kobitski, A. Yu.; Zahn, D. R. T.; Schreiber, M. *Phys. Rev. B* **2005**, *72*, 245208. (k) Scholz, R.; Schreiber, M. *Chem. Phys.* **2006**, *325*, 9.

(14) Langhals, H.; Ismael, R. *Eur. J. Org. Chem.* **1998**, 1915.

(15) Giaimo, J. M.; Gusev, A. V.; Wasielewski, M. R. *J. Am. Chem. Soc.* **2002**, *124*, 8530.

(16) (a) van der Boom, T.; Hayes, R. T.; Zhao, Y.; Bushard, P. J.; Weiss, E. A.; Wasielewski, M. R. *J. Am. Chem. Soc.* **2002**, *124*, 9582. (b) Ahrens, M. J.; Sinks, L. E.; Rybtchinski, B.; Liu, W.; Jones, B. A.; Giaimo, J. M.; Gusev, A. V.; Goshe, A. J.; Tiede, D. M.; Wasielewski, M. R. *J. Am. Chem. Soc.* **2004**, *126*, 8284.

(17) Giaimo, J. M.; Lockard, J. V.; Sinks, L. E.; Scott, A. M.; Wilson, T. M.; Wasielewski, M. R. *J. Phys. Chem. A* **2008**, *112*, 2322.

(18) Fuller, M. J.; Sinks, L. E.; Rybtchinski, B.; Giaimo, J. M.; Li, X.; Wasielewski, M. R. *J. Phys. Chem. A* **2005**, *109*, 970.

(19) Lovinger, A. J.; Forrest, S. R.; Kaplan, M. L.; Schmidt, P. H.; Venkatesan, T. *J. Appl. Phys.* **1984**, *55*, 467.

(20) Kasha, M.; Rawls, H. R.; El-Bayoumi, M. A. *Pure Appl. Chem.* **1965**, *11*, 371.

(21) (a) Deng, Y.; Chang, C. J.; Nocera, D. G. *J. Am. Chem. Soc.* **2000**, *122*, 410. (b) Kadish, K. M.; Frémond, L.; Ou, Z.; Shao, J.; Shi, C.; Anson, F. C.; Burdet, F.; Gros, C. P.; Barbe, J.-M.; Guilard, R. *J. Am. Chem. Soc.* **2005**, *127*, 5625.

(22) (a) Beens, H.; Knibbe, H.; Weller, A. *J. Chem. Phys.* **1967**, *47*, 1183. (b) Castanheira, E. M. S.; Martinho, J. M. G. *J. Photochem. Photobiol., A* **1994**, *80*, 151.

(23) Langhals, H.; Jona, W. *Chem.— Eur. J.* **1998**, *4*, 2110.

(24) Hamann, B. C.; Branda, N. R.; Rebek, J. *Tetrahedron Lett.* **1993**, *34*, 6837.

(25) Kaiser, H.; Lindner, J.; Langhals, H. *Chem. Ber.* **1991**, *124*, 529.

(26) Demol, F.; De Backer, M. G.; Levillain, E.; Sauvage, F. X. *Spectrochim. Acta A* **2001**, *57*, 1611.

(27) Oldham, K. B.; Zoski, G. D. *Anal. Chem.* **1980**, *52*, 2116.

(28) David R. Lide, Ed., *CRC Handbook of Chemistry and Physics*, 88th ed. (internet version); CRC Press/Taylor and Francis: Boca Raton, FL, 2008.

(29) Langhals, H.; Karolin, J.; Johansson, L. B.-Å. *J. Chem. Soc., Faraday Trans.* **1998**, *94*, 2919.

(30) Φ_F in 2-Me-THF, DCM, and *o*-DCB were not determined for **PDI**. However, similarly high yields as those in the other solvents have been reported for other "bare" PDIs with 2,5-di-*t*-butylphenyl solubilizing groups in a wide range of solvents (ref 10a).

(31) Gosztola, D.; Niemczyk, M. P.; Svec, W.; Lukas, A. S.; Wasielewski, M. R. *J. Phys. Chem. A* **2000**, *104*, 6545.

(32) Ware, W. R.; Watt, D.; Holmes, J. D. *J. Am. Chem. Soc.* **1974**, *96*, 7853.

(33) Φ_F was corrected for the residual structured emission, assuming a constant $\Phi_F = 0.006$ in all solvents. Without this correction, only k_F in

o-DCB would be significantly (20%) lower. The values for k_{NR} are not (<1%) affected by the correction.

(34) Leinhos, U.; Kühnle, W.; Zachariasse, K. A. *J. Phys. Chem.* **1991**, *95*, 2013.

(35) For the perylene excimer, Katoh et al. (ref 36) estimated a stabilization energy of 0.19 eV relative to the lowest exciton state.

(36) Katoh, R.; Sinha, S.; Murata, S.; Tachiya, M. *J. Photochem. Photobiol., A* **2001**, *145*, 23.

(37) (a) Williams, R. M.; Zwier, J. M.; Verhoeven, J. W. *J. Am. Chem. Soc.* **1995**, *117*, 4093. (b) Guldi, D. M.; Asmus, K.-D. *J. Phys. Chem. A* **1997**, *101*, 1472.

(38) Schmidt, R.; Afshari, E. *J. Phys. Chem.* **1990**, *94*, 4377.

(39) Scurlock, R. D.; Nonell, S.; Braslavsky, S. E.; Ogilby, P. R. *J. Phys. Chem.* **1995**, *99*, 3521.

(40) Arbogast, J. W.; Darmanyan, A. P.; Foote, C. S.; Rubin, Y.; Diederich, F. N.; Alvarez, M. M.; Anz, S. J.; Whetten, R. L. *J. Phys. Chem.* **1991**, *95*, 11.

(41) Terazima, M.; Hirota, N.; Shinohara, H.; Saito, Y. *J. Phys. Chem.* **1991**, *95*, 9080.

(42) Schmidt, R.; Tanielian, C. *J. Phys. Chem. A* **2000**, *104*, 3177.

(43) According to Schmidt et al. (ref 42), special care must be taken for TPP in benzene, as the oxygen ($^1\Delta_g$) luminescence may deviate early from linearity.

(44) As explained by Beeby et al. (ref 45), this may cause such signals that even extend to a few μs. For TPP, similar signals were reported by Schmidt et al. (ref 46).

(45) Beeby, A.; Parker, A. W.; Stanley, C. F. *J. Photochem. Photobiol., B* **1997**, *37*, 267.

(46) Schweitzer, C.; Schmidt, R. *Chem. Rev.* **2003**, *103*, 1685.

JP8022524